CrystEngComm

Cite this: *CrystEngComm*, 2012, **14**, 8253–8260

www.rsc.org/crystengcomm

PAPER

Novel synthesis and formation process of uniform Mn_2O_3 cubes†

Jianfang Wang,[ab] Gang Zhu,[ab] Lingjuan Deng,[ab] Liping Kang,[ab] Zhengping Hao[c] and Zonghuai Liu*[ab]

Received 21st July 2012, Accepted 14th September 2012
DOI: 10.1039/c2ce26176f

Uniform Mn_2O_3 cube with an average particle size of 4 μm is synthesized *via* a hydrothermal treatment of H-type layered manganese oxide in tetramethylammonium hydroxide (TMAOH) solution at 180 °C for 24 h. The as-prepared materials are characterized by XRD, SEM, TEM, XPS, TG-DTA, and IR and the formation process of Mn_2O_3 cubes is also investigated. TMA^+ ions play an important role for the formation of Mn_2O_3 with good crystallinity and regular cubic morphology. The intercalation of TMA^+ ions into the layered manganese oxide firstly causes a short-range swelling expansion of the interlayer, and the swelled layered manganese oxide is exfoliated into their elementary host sheets by a hydrothermal treatment. Some Mn(III) probably migrates into the solution and Mn(IV) is reduced by methanol decomposed by TMAOH in the hydrothermal system, and forms Mn_2O_3 crystal nuclei under suitable hydrothermal condition. TMA^+ ions in the solution are selectively adsorbed on the (100) planes of Mn_2O_3 crystal nucleus, and finally generates Mn_2O_3 particles with cubic morphology.

1. Introduction

In recent years, the controllable synthesis of nano- or microsized transition metal oxides with different morphologies has attracted considerable interest because their properties depend on not only their chemical composition, but also their structure, morphology, dimension and size distribution.[1–4] In particular, the assembling fabrication of the transition metal oxides with different morphologies has been widely utilized in various fundamental research and technological applications, and the fabricated materials show promising applications in energy storage, catalysis, gas sensing, separation and bio-diagnostic sensing.[5–7] Among the transition metal oxides, manganese oxides are given wide attention because of their special physical and chemical properties and potential applications in catalysis, ion exchange, molecular adsorption, and energy storage in lithium ion secondary battery and supercapacitor.[8–12]

Research results show that the morphology of manganese oxides connects with their surface area, density, and surface to volume ratio, which have an obvious effect on their physical and chemical properties.[9–11] Therefore, the controllable fabrication of the manganese-based materials with different morphologies is important from the viewpoint of the foundational research and technological application. Many efforts have been devoted to the synthesis of manganese-based materials with different morphologies.[12–15] Mn_2O_3 is a traditionally attractive material for various industrial applications, such as a cheap and environmentally-friendly catalyst for removing carbon monoxide and nitrogen oxide from waste gas,[16–18] the precursor for producing soft magnetic materials,[19] and the electrode material of rechargeable lithium batteries.[20] Up to now, a wide variety of Mn_2O_3 with different morphologies, ranging from one to three-dimensional structures, such as rods, wires, cubes, octahedra, and hollow spheres, have been synthesized through various methods. Porous one-dimensional Mn_2O_3 nanostructures are fabricated *via* hydrothermal and solvothermal treatment.[21] α-Mn_2O_3 nanorods are synthesized using $KMnO_4$ as manganese source and CTAB as reducing regent,[22] and also α-Mn_2O_3 with cubic morphology can be prepared by a sol–gel process.[23] The orthorhombic phase of Mn_2O_3 octahedral nanoparticles are synthesized by a mediated *N*,*N*-dimethylformamide (DMF).[24] Cubic Mn_2O_3 hollow structures are obtained by oxidizing $MnCO_3$ microspheres, microcubes, and microellipsoids with $KMnO_4$ and then followed by calcining.[25] Although many efforts have been made to synthesize Mn_2O_3 with different morphologies, the controlled synthesis of Mn_2O_3 cube with microsized particle is still a challenge.

Layered manganese oxide is excellent precursor for preparing other manganese-based materials. Research results indicate that layered manganese oxide can be delaminated into their elementary host sheets and also can be transformed to other manganese oxides with different morphologies and structures, such as α-MnO_2,[26] β-MnO_2,[27] MnO_2 nanotube[13,28] *etc.* under suitable conditions. In view of the experimental results that layered manganese oxide can be delaminated into their elementary host nanosheets and then transformed to other

[a]*Key Laboratory of Applied Surface and Colloid Chemistry (Shanxi Normal University), Ministry of Education, Xi'an, 710062, P. R. China. E-mail: zhliu@snnu.edu.cn; Fax: +86-29-81530702; Tel: +86-29-81530716*
[b]*School of Materials Science and Engineering, Shanxi Normal University, Xi'an, 710062, P. R. China*
[c]*Research Center for Eco-Environmental Sciences, Chinese Academy of Sciences, Beijing, 100085, P. R. China*
† Electronic supplementary information (ESI) available: See DOI: 10.1039/c2ce26176

manganese oxides with different morphologies and structures, a new method is developed for synthesizing Mn_2O_3 microcubes with a particle size of 2–5 μm *via* hydrothermal treating layered manganese oxides in TMAOH aqueous solution, and the formation process of Mn_2O_3 microcubes is also investigated.

2. Experimental section

2.1. Materials

All chemicals are of analytical grade, used without further purification. Sodium hydroxide (96%), hydrogen peroxide solution (30%), concentrated hydrochloric acid, and manganese nitrate (50%) were purchased from Sinopharm Group Co. Ltd. TMAOH solution (25%) was purchased from Alfar-Aesar.

2.2. Sample synthesis

The precursor, layered manganese oxide was prepared as reported in the literature.[29] A mixed solution of 0.6 M NaOH and 2 M H_2O_2 was poured quickly into 0.3 M $Mn(NO_3)_2$ solution and stirred for 25 min. The precipitate was then subjected to hydrothermal treatment at 150 °C for 16 h in 2 M NaOH solution, Na-type layered manganese oxide was obtained. Na-type layered manganese oxide was treated with 0.1 M HCl solution at room temperature for 3 d to produce a proton-type layered manganese oxide, which was abbreviated as BirMO(H).

A typical synthesis procedure of Mn_2O_3 cubes was as follows: 0.5 g BirMO(H) was soaked in TMAOH solution (0.14 M, 21 ml) and stirred for 30 min, the obtained suspension was then transferred into a Teflon-lined stainless steel autoclave of capacity 25 ml. After the autoclave was maintained at 180 °C for 24 h and cooled naturally to room temperature, the resulting precipitate was filtered, thoroughly washed with distilled water three times and dried at 50 °C for 24 h in air, Mn_2O_3 cubes were obtained. The effect of the TMAOH concentration, the hydrothermal reaction temperature and reaction time on the morphology and crystallinity of the obtained products was investigated by the above same procedure.

2.3. Characterization

The X-ray diffraction pattern was measured on a D/Max-3c X-ray diffractometer with Cu Kα (λ = 1.5406 Å), using an operation voltage and current of 40 kV and 30 mA, respectively. The scanning electron microscopy (SEM) images were taken using a TM 3000 tabletop microscope. The high-resolution transmission electron microscopy (HRTEM) images were captured on JEM-2100 instrument. The X-ray photoelectron spectra (XPS) were recorded with a K-Alpha spectrometer using Al Kα radiation (1486.6 eV) at a power of 150 W (accelerating voltage at 12 kV and current at 6 mA) in a vacuum of 8.0×10^{-8} mPa. The binding energy reference was taken at 284.6 eV for the C 1s peak arising from surface hydrocarbons. Infrared spectra were obtained by the KBr method on a Fourier Transform Infrared Spectrometer EQUINX55. Thermal analysis was determined on DSC-TGA analysis (Q1000DSC + LNCS + FACS Q600SDT) at a heating rate of 10 °C min^{-1} from 25 °C to 1100 °C under air atmosphere.

3. Results and discussion

3.1. Structure and morphology of Mn_2O_3 cube

The XRD patterns of the samples obtained at different stages are shown in Fig. 1. Precursor BirMO(H) shows two obvious diffraction peaks at around 12.3° (001 planes) and 24.6° (002 planes), suggesting that the prepared precursor, BirMO(H), belongs to δ-type crystal with a layered structure and a basal spacing of 0.73 nm, with crystal water and exchangeable H^+ ions in the interlayer space (Fig. 1a).[30] The precursor BirMO(H) is soaked in 0.14 M TMAOH solution and stirred for 30 min, the obtained suspension is then transferred into a Teflon-lined stainless steel autoclave. After the autoclave is maintained at 180 °C for 30 min, the XRD pattern for the obtained material gives no clear peaks but only an amorphous halo in contrast to that of BirMO(H) (Fig. 1b). The halo can be interpreted as scattering from the manganese oxide nanosheets which are aggregated irregularly, similar to the case of layered titanic acid or graphite oxide.[31] This result indicates that the stacked layered manganese oxide plates are delaminated into the individual primary plates under the present condition, similar to that of BirMO(H) treated in TMAOH solution (0.35 M) for 7 days at room temperature.[32] After prolonging the hydrothermal treatment time to 24 h, all of the diffraction peaks of the as-synthesized material can be perfectly indexed to the cubic bixbyite α-Mn_2O_3 (JCPDS, No.41-1442, a = 9.409 Å) (Fig. 1c). No peaks from other phases are found, suggesting that the as-synthesized Mn_2O_3 has high purity. These results suggest that Mn_2O_3 can be effectively prepared when the precursor, BirMO(H), is treated hydrothermally in 0.14 M TMAOH solution at 180 °C for 24 h.

SEM image of the precursor BirMO(H) shows an irregular plate-like morphology with a thickness less than 0.1 μm (Fig. 2a), while the material obtained by treating BirMO(H) in 0.14 M

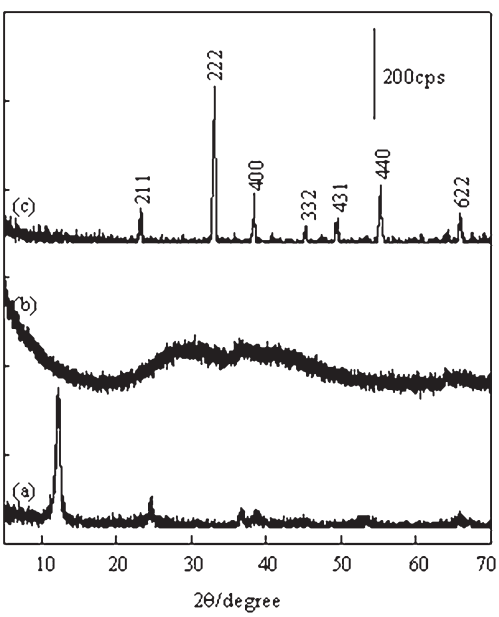

Fig. 1 XRD patterns of the obtained samples: (a) BirMO(H), (b) the material obtained by hydrothermal treating BirMO(H) at 180 °C for 30 min, and (c) Mn_2O_3 cubes.

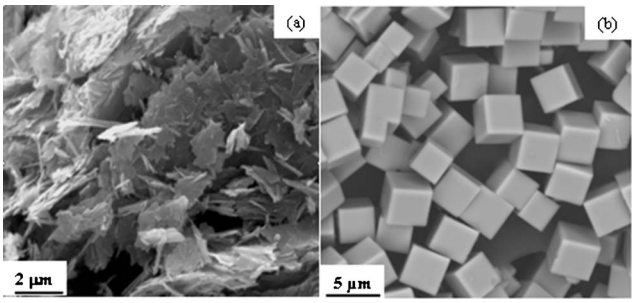

Fig. 2 SEM images of samples: (a) BirMO(H) and (b) Mn_2O_3 cubes.

TMAOH solution at 180 °C for 24 h is dominated by Mn_2O_3 cube with an edge length of 2–5 μm (Fig. 2b). SEM images suggest that the hydrothermal treatment of the precursor BirMO(H) in TMAOH solution causes the formation of Mn_2O_3 with cubic morphology. The oval-shaped cubic Mn_2O_3 is observed clearly by transmission electron microscopy (TEM) observation (Fig. 3a), and the side length of Mn_2O_3 particles is about 4 μm. The high-resolution lattice image from one region of Mn_2O_3 cube shows continuous and clear lattice fringes in a single microcube, indicating high crystallinity of the obtained Mn_2O_3 cube (Fig. 3b). The pattern of an individual cube particle of Mn_2O_3 exhibits general spots, confirming the single-crystal nature. The lattice spacing of 0.47 nm and 0.27 nm is recognized and corresponds to the inter-plane distances of (200) and (222) of the α-Mn_2O_3, respectively (Fig. 3c).

3.2. Effect of the reaction conditions on the morphology and structure of the obtained materials

On the basis of the above experimental results, it can be concluded that TMA^+ ions play an important role for the formation of Mn_2O_3 with good crystallinity and regular cubic morphology. Without the addition of TMA^+ ions into the reaction system, the SEM image of the obtained product hardly shows regular morphology, which is very different from those of samples obtained by the addition of TMA^+ ions (Fig. 4a). On the other hand, the morphology of the obtained materials depends on the concentration of TMA^+ ions added into the reaction system. With the increasing of TMA^+ ion concentration (c), the morphology of the obtained materials obviously changes. Up to c (TMA^+) = 0.07 M, particles with platelike and rodlike mixed morphology are mainly observed with a little cubic morphology (Fig. 4b). Further increasing TMA^+ ion concentration to 0.14 M, Mn_2O_3 with uniform cubic morphology only are obtained (Fig. 4c). A mainly cubic morphology with a little rodlike morphology is observed when TMA^+ ion concentration increases to 0.21 M (Fig. 4d). These results indicate that an optimal TMA^+ ion concentration is favorable for the formation of Mn_2O_3 cube, and the optimized concentration of TMA^+ ion is about 0.14 M.

The effect of the hydrothermal treatment temperature on the morphology of the obtained materials is studied at c (TMA^+) = 0.14 M for 24 h. SEM morphologies of the materials obtained at different hydrothermal temperatures at c (TMA^+) = 0.14 M for 24 h are shown in Fig. 5. It can be seen that the morphology, size, and uniformity of the as-prepared materials are connected with the hydrothermal treatment temperatures, and uniform Mn_2O_3 cube with a mean lateral size of 4 μm is obtained at 180 °C (Fig. 5b). On the other hand, uniform Mn_2O_3 cube is not obtained when the hydrothermal treatment temperature is below or above 180 °C. The uniform Mn_2O_3 cube is destroyed to small irregular particles above 220 °C (Fig. 5c) although the obtained sample has a good crystallinity. Therefore, Mn_2O_3 with uniform cubic morphology can be obtained at 180 °C for 24 h when c (TMA^+) = 0.14 M.

3.3. Formation process of Mn_2O_3 cube

The above experimental results indicate that the TMA^+ ions play a key role for the formation of Mn_2O_3 with uniform cubic

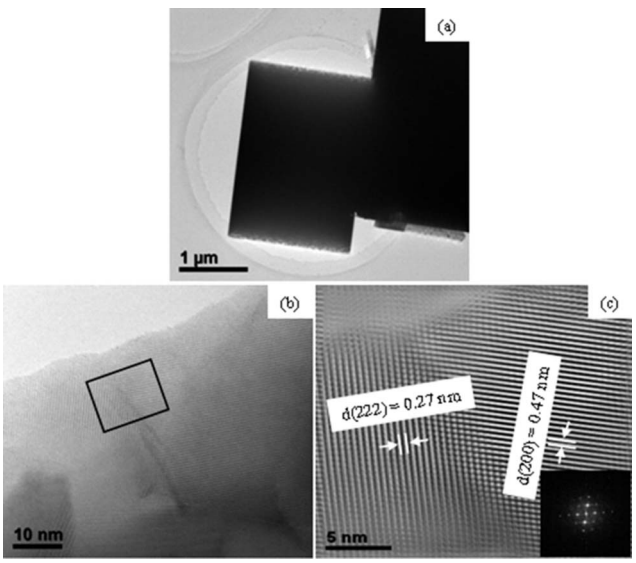

Fig. 3 TEM image of Mn_2O_3 cubes (a), an enlarged TEM image taken from its edge of an over-shaped Mn_2O_3 (b), and HRTEM image taken from (b) (marked with a square symbol) and its corresponding FFT pattern (inset) (c).

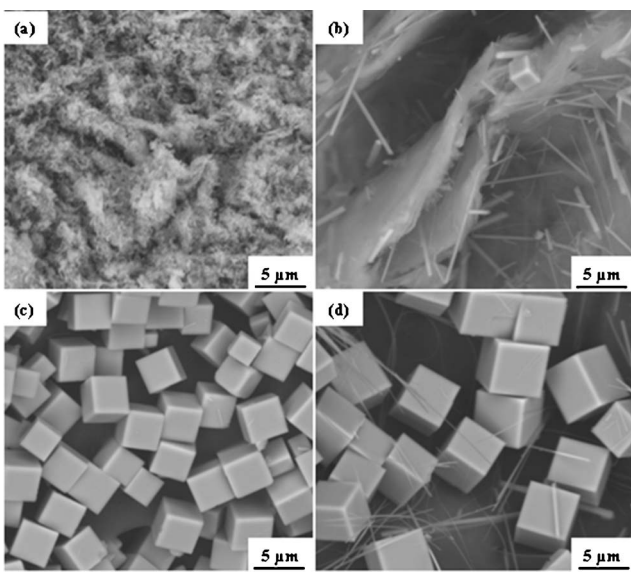

Fig. 4 SEM images of the obtained materials at different concentrations of TMAOH at 180 °C: (a) 0 M, (b) 0.07 M, (c) 0.14 M, and (d) 0.21 M.

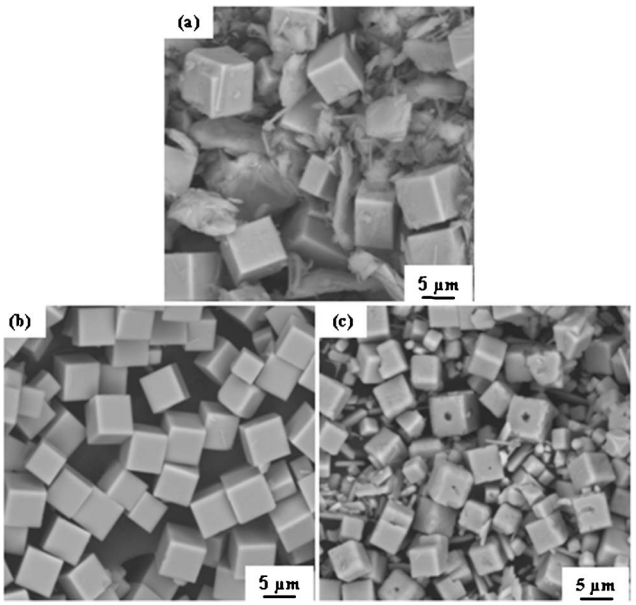

Fig. 5 SEM images of the obtained materials at different hydrothermal temperatures: (a) 160 °C, (b) 180 °C, and (c) 220 °C.

morphology at suitable hydrothermal treatment temperature and time. Therefore, it is important to know the function of TMA^+ ions and the formation process of Mn_2O_3 with uniform cubic morphology. By hydrothermal treating in TMAOH solution at 180 °C for 3 h, the layered structure is almost maintained, only the basal spacing is enlarged from 0.73 nm to 0.96 nm due to the intercalation of TMA^+ ions into the manganese oxide interlayer

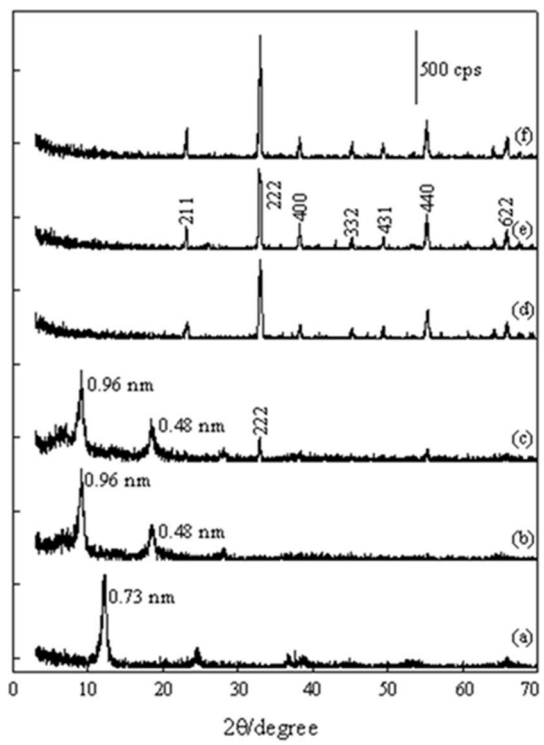

Fig. 6 XRD patterns of the obtained materials at different hydrothermal times: (a) 0 h, (b) 3 h, (c) 6 h, (d) 17 h, (e) 24 h, and (f) 48 h.

(Fig. 6b).[33] It is worth noting that a new peak appears at $2\theta = 32.9°$ as well the characteristic peaks of the precursor, BirMO(H), which is corresponding to (222) face of Mn_2O_3 cube. These results indicate that Mn_2O_3 cube begins to form by inducing TMA^+ ions when the hydrothermal treatment time prolongs to 6 h (Fig. 6c). Prolonging the hydrothermal treatment time to 17 h, the layered structure of the precursor BirMO(H) disappears completely, while a new phase is formed. All the diffraction peaks of the new phase can be indexed to α-Mn_2O_3, indicating that cubic bixbyite α-Mn_2O_3 can be obtained by hydrothermal treatment BirMO(H) at 180 °C for 17 h (Fig. 6d). Further prolonging the hydrothermal treatment times for 24 h and 48 h, only the crystallinity of the obtained materials improves, while the phase structure does not change (Fig. 6e and f, respectively).

The SEM images are also used to observe the morphology changes of the obtained materials, and the results are shown in Fig. 7. It can be seen that the precursor, BirMO(H) has a plate-like morphology (Fig. 7a). Prolonging the hydrothermal treatment time to 3 h, the plate-like morphology of BirMO(H) is nearly maintained (Fig. 7b). After hydrothermal treating for 6 h, the plate-like morphology of BirMO(H) becomes irregular and the amount of Mn_2O_3 with cubic morphology increases (Fig. 7c), which is consistent with the result of the XRD pattern (Fig. 6c). Almost cubic morphology only is observed when the hydrothermal treatment time increases to 17 h, but the uniformity of the cubic morphology is irregular (Fig. 7d), indicating that the precursor, BirMO(H) with plate-like morphology transforms completely into the α-Mn_2O_3 with cubic morphology. The α-Mn_2O_3 with uniform cubic morphology is obtained when BirMO(H) is hydrothermally treated in TMAOH solution at 180 °C for 24 h (Fig. 7e). On the basis of the XRD patterns and SEM images, it can be concluded that when the precursor, BirMO(H) is hydrothermally treated in TMAOH solution (0.14 M) at 180 °C for 24 h, it can be transformed into Mn_2O_3 with uniform cubic morphology.

The effect of the reaction time on the average diameter of Mn_2O_3 cubic particle is shown in Fig. 8. It can be observed that the increase of Mn_2O_3 cubic particle size gradually slows down as the reaction time prolongs. This kind of transformation is coincident with the change of the growth mechanism from oriented aggregation to Ostwald ripening. Gao *et al.* have found that the surfactant CTAB plays an important role in the formation process of α-Fe_2O_3 submicron-cube with high uniformity,[34] and also they have reported that the functional molecules on the surface of nanoparticles have an important influence on their self-assembly behavior.[35] The selective adsorption of organic surfactants on particular crystallographic facets has been an effective way to control the size and shape of the crystals, which would be an immense step forward towards the controlled, bottom-up fabrication of well-defined structures. In the present work, TMA^+ ions would be selectively adsorbed on the surface of Mn_2O_3 crystals depending on their different surface energies. The organic additive on different facets of the crystal would confine the growth of certain planes, which eventually would lead to oriented attachment and anisotropic growth of polyhedral symmetry structure. A contrasting experiment indicates that particles with no definite morphology are obtained when TMA^+ ions are not added in the reaction system

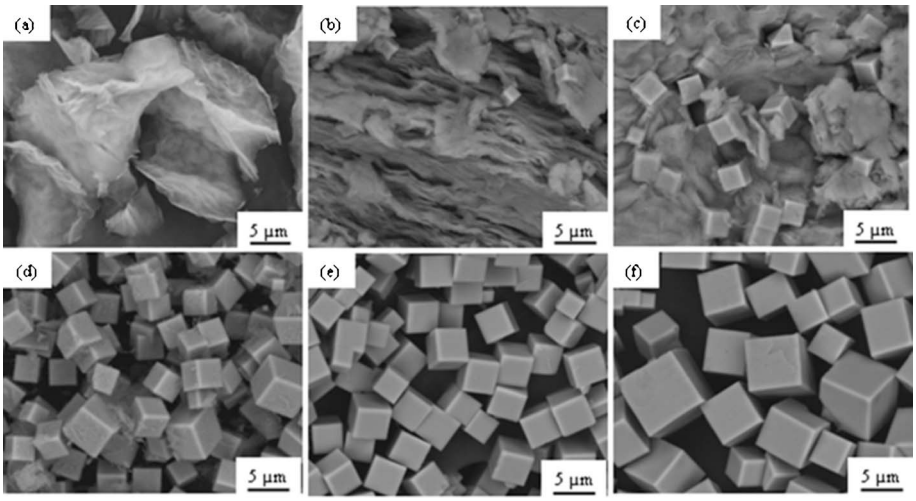

Fig. 7 SEM images of the obtained materials at different hydrothermal times: (a) 30 min, (b) 3 h, (c) 6 h, (d) 17 h, (e) 24 h, and (f) 48 h.

under the same reaction conditions (Fig. 4a), which confirms that when the particles are not restricted by the functional surfactant TMA^+ ions, they would grow randomly and aggregate in an isotropic way to form polycrystalline particles with no definite morphology. The particle size is measured by image analysis method from SEM images[36,37] and the histogram of the particle size distribution is shown in Fig. S1, ESI.† It can be seen that the obtained particles show relatively narrow size distribution with an average particle size of 3.6 μm prolonging the reaction time from 6 h to 24 h, and the growth of particles follows Ostwald ripening proceed by a dissolution–crystallization mechanism.

The Mn valence of the obtained materials during the reaction is characterized by X-ray photoelectron spectroscopy (XPS), and the Mn 3s and O 1s core level spectra are shown in Fig. 9. It can be seen that the energy separation data (ΔE) between the two peaks of the Mn 3s core level spectra is 4.59, 4.96, 5.13, and 5.42 eV, respectively for the materials obtained at 30 min, 6 h, 17 h, and 24 h (Fig. 9, left). These values are in good agreement with the literature data, which are 5.79, 5.50, 5.41, and 4.78 eV for samples: MnO, Mn_3O_4, Mn_2O_3, and MnO_2, respectively,[38] suggesting that the Mn valences of the obtained materials during the reaction are decreasing step by step. On the basis of the fitting curve of O 1s core level spectra (Fig. 9, right), the mean manganese oxidation state can be estimated.[39] For the material obtained by treating hydrothermal BirMO(H) in TMAOH solution for 30 min, its mean manganese oxidation state is about 3.9, while the mean manganese oxidation state is 3.0 for the target material, Mn_2O_3. These results indicate that the target material, Mn_2O_3 is formed completely after BirMO(H) is treated hydrothermally in TMAOH solution for 24 h. The rate of the nucleus formation accompanied by the reduction of Mn^{4+} to Mn^{3+} is slower than that in the conventional solution system, and the smaller nucleus formation is advantageous to the formation of Mn_2O_3 cubes.

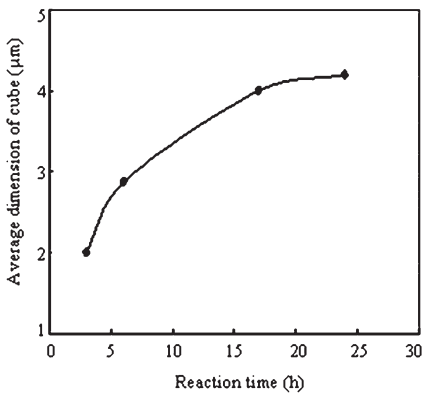

Fig. 8 Effect of reaction time on the average size of cubic Mn_2O_3 particle.

The TG and DTA curves of the obtained materials during the hydrothermal treatment process are shown in Fig. 10. Except for the weight loss of 3.9% up to 120 °C due to the evaporation of the interlayer water, two weight change stages are observed for the obtained materials. One is the obvious weight loss stage from 120 to 350 °C for materials obtained for 30 min, 3 h, and 6 h, corresponding to the decomposition of TMA^+ ions in the interlayer in addition to the partial destruction of the manganese oxide nanosheets, and the weight loss gradually decreases along with the reaction time. The weight loss is associated with a sharp exothermic peak around 240 °C, which is similar to that of the decomposition temperature of TMA^+ ions. No obvious weight loss stage from 120 to 350 °C was observed for materials obtained for 17 h and 24 h due to no decomposition of TMA^+ ions. A small weight loss between 420 and 600 °C is due to the reduction of manganese from tetravalent to trivalent form accompanied by the evolution of oxygen, which corresponds to a weak exothermic peak around 570 °C.[40] In addition, the weight loss from 940 to 1030 °C is mainly attributed to the transformation from α-Mn_2O_3 to Mn_3O_4.[41] The transformation process is also supported by IR spectra of the obtained materials during the hydrothermal treatment reaction, and the experimental results are shown in Fig. S2, ESI.† The characteristic absorption bands of TMA^+ ions in the interlayer at 1487 and 948 cm^{-1} can be observed for the materials obtained for 30 min, 3 h, and 6 h,[42] while these absorption bands are not found for the materials obtained for 17 h and 24 h due to the remove of TMA^+ ions. The IR bands around 700–400 cm^{-1} are ascribed to the absorption

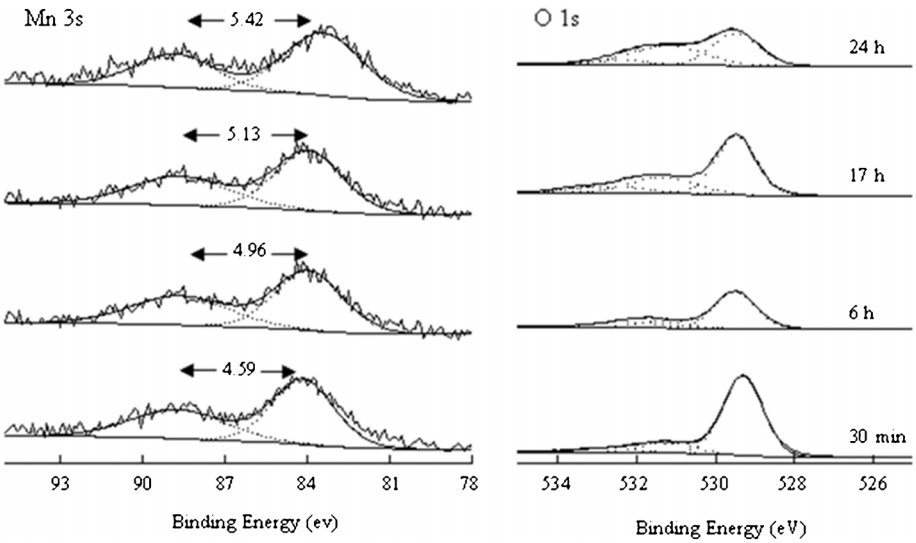

Fig. 9 Mn 3s core level spectra (left) and O 1s core level spectra (right) of the obtained materials at different hydrothermal treatment times.

by Mn–O lattice vibrations.[43] In particular, the diagnostic absorption bands of α-Mn_2O_3 (at 668, 573, 525, and 473 cm^{-1}) are well-represented in the spectra of the obtained samples for 17 h and 24 h.[44] These results clearly indicate that TMA^+ ions play an important role in the transformation from layered manganese oxide to Mn_2O_3, and the Mn_2O_3 cubes are completely formed after prolonging the hydrothermal treatment reaction time to 24 h, which is consistent with the SEM images and XRD patterns.

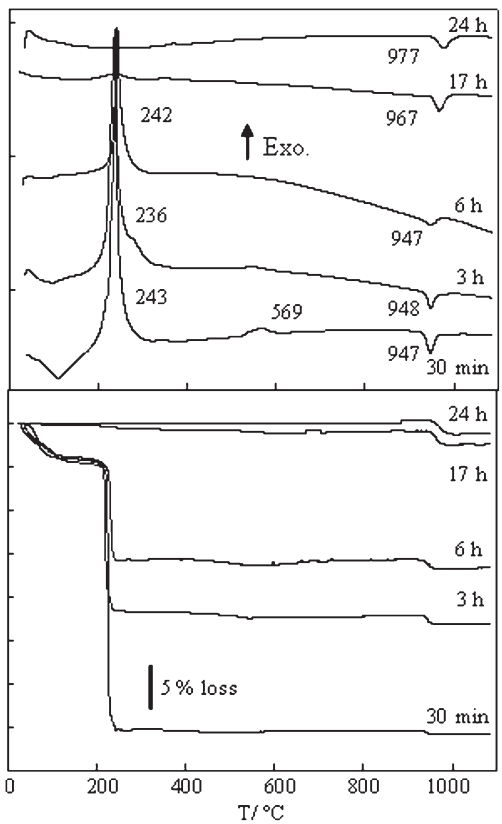

Fig. 10 TG and DTA curves of the obtained materials during the hydrothermal treatment process.

On the basis of the above experimental results, a formation process of Mn_2O_3 with uniform cubic morphology is presented in Fig. 11. At first, the intercalation of TMA^+ ions into the layered manganese oxide causes a short-range swelling expansion of the interlayer,[43] and a layered manganese oxide with a basal spacing of 0.96 nm is obtained. In general, the short range swelling is controlled mainly by the three forces acting between the neighboring sheets; the electrostatic attractive force between the interlayer cation and negatively charged sheet, the repulsive force caused by hydration of the interlayer cation, and the attractive force caused by hydrogen bonding between the oxide sheet and water molecules.[32] Therefore, the intercalation of large TMA^+ cations eliminates a considerable number of water molecules from the interlayer to reduce the number of hydrogen bonds; thus the swelling becomes possible with an appropriate TMA^+ content, due to the strong repulsive force by hydration of TMA^+ ions. The swelled layered manganese oxide is hydrothermally treated in TMAOH solution at 180 °C, the layered structure is exfoliated into their elementary host sheets.[45] These manganese oxide nanosheets, which have a large specific surface area and high surface energy, and show high reactive property, are formed by edge-shared MnO_6 octahedra with mixed Mn(IV) and Mn(III) octahedral.[46] The formation process of Mn_2O_3 cube is relatively complex because it contains both the ion exchange (H^+/TMA^+) and redox (Mn^{4+} to Mn^{3+}) reactions in aqueous TMAOH medium under hydrothermal condition.[13,47] Under the hydrothermal treatment condition in TMAOH solution, some Mn(III) probably migrate into the solution and Mn(IV) are reduced by methanol on the delaminated manganese oxide nanosheets, and forms Mn_2O_3 crystal nucleus under suitable hydrothermal condition. TMA^+ ions in the solution are selectively adsorbed on the (100) planes of Mn_2O_3 crystal nuclei, and finally generate Mn_2O_3 particles with cube morphology.

4. Conclusion

In summary, a novel preparation method of uniform Mn_2O_3 cube with an average particle size of 4 μm is developed by a

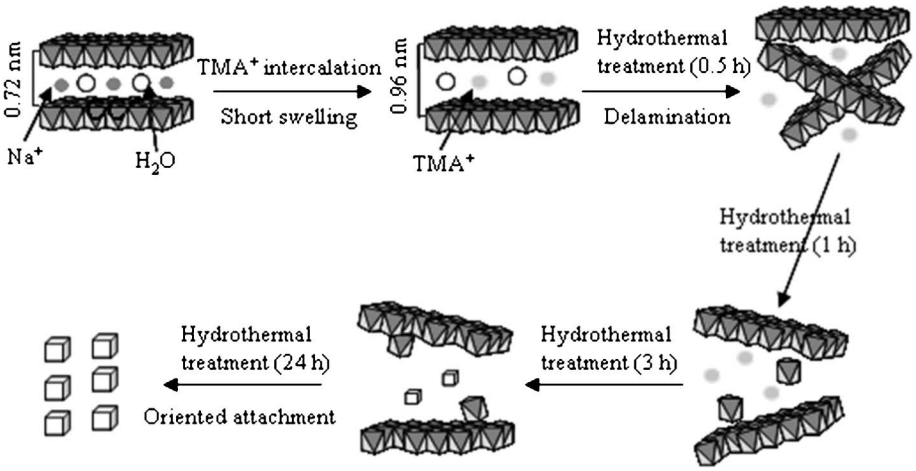

Fig. 11 The formation process of Mn_2O_3 with uniform cubic morphology.

hydrothermal treatment of H-type layered manganese oxide in TMAOH solution. TMA^+ ions play an important role for the formation of Mn_2O_3 with good crystallinity and regular cubic morphology. TMA^+ ions not only result in the delamination of layered manganese oxide, but also are selectively adsorbed on the (100) planes of Mn_2O_3 crystal nucleus, and finally generate Mn_2O_3 particles with cubic morphology. The layered manganese oxide is a fundamental and potential precursor to synthesis manganese oxides materials with novel morphologies and crystal phases.

Acknowledgements

This work was supported by the National Natural Science Foundation of China (51172137), the Natural Science Key Foundation of Shanxi Province (2011JZ001), Changjiang Scholars and Innovative Research Team in University (IRT1070) and the Fundamental Research Funds for the Central Universities (GK201001001).

References

1 X. Peng, L. Manna, W. Yang, J. Wickham, E. Scher, A. Kadavanich and A. P. Alivisatos, *Nature*, 2000, **404**, 59.
2 C. Petit, A. Taleb and M. P. Pileni, *Adv. Mater.*, 1998, **10**, 259.
3 J. T. Han, Y. H. Huang, X. J. Wu, C. L. Wu, W. Wei, B. Peng, W. Huang and J. B. Goodenough, *Adv. Mater.*, 2006, **18**, 2145.
4 J. Chen, L. N. Xu, W. Y. Li and X. L. Gou, *Adv. Mater.*, 2005, **17**, 582.
5 C. K. King'ondu, A. Iyer, E. C. Njagi, N. Opembe, H. Genuino, H. Huang, R. A. Ristau and S. L. Suib, *J. Am. Chem. Soc.*, 2011, **133**, 4186.
6 L. P. Xu, Y. S. Ding, C. H. Chen, L. L. Zhao, C. Rimkus, R. Joesten and S. L. Suib, *Chem. Mater.*, 2008, **20**, 308.
7 L. Q. Mai, L. Xu, C. H. Han, X. Xu, Y. Z. Luo, S. Y. Zhao and Y. L. Zhao, *Nano Lett.*, 2010, **10**, 4750.
8 W. Xiao, D. L. Wang and X. W. Lou, *J. Phys. Chem. C*, 2010, **114**, 1694.
9 R. Koivula, J. Pakarinen, M. Sivenius, K. Sirola, R. Harjula and E. Paatero, *Sep. Purif. Technol.*, 2009, **70**, 53.
10 Y. Zhai, J. Zhai, M. Zhou and S. Dong, *J. Mater. Chem.*, 2009, **19**, 7030.
11 J. Zhao, Z. Tao, J. Liang and J. Chen, *Cryst. Growth Des.*, 2008, **8**, 2799.
12 H. Jiang, T. Zhao, J. Ma, C. Y. Yan and C. Z. Li, *Chem. Commun.*, 2011, **47**, 1264.
13 L. H. Li, C. Y. Nan, J. Lu, Q. Peng and Y. D. Li, *Chem. Commun.*, 2012, **48**, 6945.
14 S. Ching, D. A. Kriz, K. M. Luthy, E. C. Njagi and S. L. Suib, *Chem. Commun.*, 2011, **47**, 8286.
15 M. Fang, X. L. Tan, M. Liu, S. H. Kang, X. Y. Hu and L. D. Zhang, *CrystEngComm*, 2011, **13**, 4915.
16 S. Imamura, M. Shono, N. Okamoto, A. Hamada and S. Ishida, *Appl. Catal., A*, 1996, **142**, 279.
17 B. T. Ji, X. L. Jiao, N. Sui, Y. Z. Duan and D. R. Chen, *CrystEngComm*, 2010, **12**, 3229.
18 L. C. Wang, L. He, Y. M. Liu, Y. Cao, H. Y. He, K. N. Fan and J. H. Zhuang, *J. Catal.*, 2009, **264**, 145.
19 T. Ahmad, K. V. Ramanujachary, S. E. Loflandb and A. K. Ganguli, *J. Mater. Chem.*, 2004, **14**, 3406.
20 F. Jiao, J. L. Bao, A. H. Hill and P. G. Bruce, *Angew. Chem., Int. Ed.*, 2008, **47**, 1.
21 Y. Cai, S. Liu, X. M. Yin, Q. Y. Hao, M. Zhang and T. H. Wang, *Phys. E.*, 2010, **43**, 70.
22 Y. C. Chen, Y. G. Zhang, Q.-Z. Yao, G.-T. Zhou, S. Q. Fu and H. Fan, *J. Solid State Chem.*, 2007, **180**, 1218.
23 D. Ramarajan and P. Sivagurunathan, *J. Solid State Chem.*, 2011, **184**, 597.
24 L. Liu, H. Liang, H. X. Yang, J. J. Wei and Y. Z. Yang, *Nanotechnology*, 2011, **22**, 015603.
25 J. Cao, Y. C. Zhu, K. Y. Bao, L. Shi, S. Z. Liu and Y. T. Qian, *J. Phys. Chem. C*, 2009, **113**, 17755.
26 L. C. Zhang, L. P. Kang, H. Lv and Z. K. Su, *J. Mater. Res.*, 2008, **23**, 780.
27 L. C. Zhang, Z.-H. Liu, X. H. Tang, J. F. Wang and K. Ooi, *Mater. Res. Bull.*, 2007, **42**, 1432.
28 R. Z. Ma, Y. Bando and T. Sasaki, *J. Phys. Chem. B*, 2004, **108**, 2115.
29 Q. Feng, E. H. Sun, K. Yanagisawa and N. Yamasaki, *J. Ceram. Soc. Jpn.*, 1995, **7**, 1722.
30 D. S. Yang and M. K. Wang, *Chem. Mater.*, 2001, **13**, 2589.
31 T. Sasaki and M. Watanabe, *J. Am. Chem. Soc.*, 1998, **120**, 4682.
32 Z.-H. Liu, K. Ooi, H. Kanoh, W. P. Tang and T. Tomida, *Langmuir*, 2000, **16**, 4154.
33 Z. P. Liu, R. Z. Ma, Y. Ebina, K. Takada and T. Sasaki, *Chem. Mater.*, 2007, **19**, 6504.
34 B. P. Jia and L. Gao, *Cryst. Growth Des.*, 2008, **8**, 1372.
35 H. L. Cao, X. F. Qian, C. Wang, X. D. Ma, J. Yin and Z. K. Zhu, *J. Am. Chem. Soc.*, 2005, **127**, 16024.
36 J. Spadavecchia, S. Casale, S. Boujday and C.-M. Pradier, *Colloids Surf., B*, 2012, **100**, 1.
37 M. Chen, C. Y. Ma, T. Mahmud, T. Lin, X. Z. Wang, *Particulate Materials: Synthesis, Characterisation, Processing and Modelling*, 2011, p. 28.
38 M. Chigane and M. Ishikawa, *J. Electrochem. Soc.*, 2000, **147**, 2246.
39 M. Toupin, T. Brousse and D. Bélanger, *Chem. Mater.*, 2004, **16**, 3184.
40 Q. Feng, H. Kanoh, Y. Miyai and K. Ooi, *Chem. Mater.*, 1995, **7**, 1722.

41 E. R. Stobbe, B. A. de Boer and J. W. Geus, *Catal. Today*, 1999, **47**, 161.
42 Z.-H. Liu, X. J. Yang, Y. Makita and K. Ooi, *Chem. Mater.*, 2002, **14**, 4800.
43 X. J. Yang, Y. Makita, Z.-H. Liu, K. Sakane and K. Ooi, *Chem. Mater.*, 2004, **16**, 5581.
44 M. I. Zaki, M. A. Hasan, L. Pasupulety and K. Kumari, *New J. Chem.*, 1998, **22**, 875.
45 K. Fukuda, I. Nakai, Y. S. Ebina, M. Tanaka, T. Mori and T. Sasaki, *J. Phys. Chem. B*, 2006, **110**, 17070.
46 Q. Feng, K. Hirofumi, Y. Miyai and K. Ooi, *Chem. Mater.*, 1995, **7**, 1226.
47 W.-N. Li, L. C. Zhang, S. Sithambaram, J. K. Yuan, X.-F. Shen, M. Aindow and S. L. Suib, *J. Phys. Chem. C*, 2007, **111**, 14694.